

Keeping a quantum bit alive by feed-forward decoupling

Authors

G. Braunbeck¹, M. Kaindl¹, A. M. Waeber¹, F. Reinhard^{1,*}

¹Walter Schottky Institut and Physik Department, Technische Universität München, Am Coulombwall 4, 85748 Garching, Germany

*friedemann.reinhard@wsi.tum.de

Abstract

We present “feedforward decoupling”, a scheme to protect a qubit against pure dephasing induced by noise of a classical environment. The scheme builds upon the key idea that this kind of noise can be recorded by a classical device during the qubit evolution, and that its effect can be undone by a suitable control sequence that is conditioned on the measurement result. We specifically demonstrate this scheme on a nitrogen-vacancy (NV) center that strongly couples to current noise in a nearby conductor. By conditioning the readout observable on a measurement of the current, we recover the full qubit coherence and the qubit’s intrinsic coherence time T_2 . We demonstrate that this scheme provides a simple way to implement single-qubit gates with an infidelity of 10^{-2} even if they are driven by noisy sources, and we estimate that an infidelity of 10^{-5} could be reached with additional improvements. We anticipate this method to find widespread adoption in experiments using fast control pulses driven from strong currents, in particular in nanoscale magnetic resonance imaging, where control of peak currents of 100 mA with a bandwidth of 100 MHz is required.

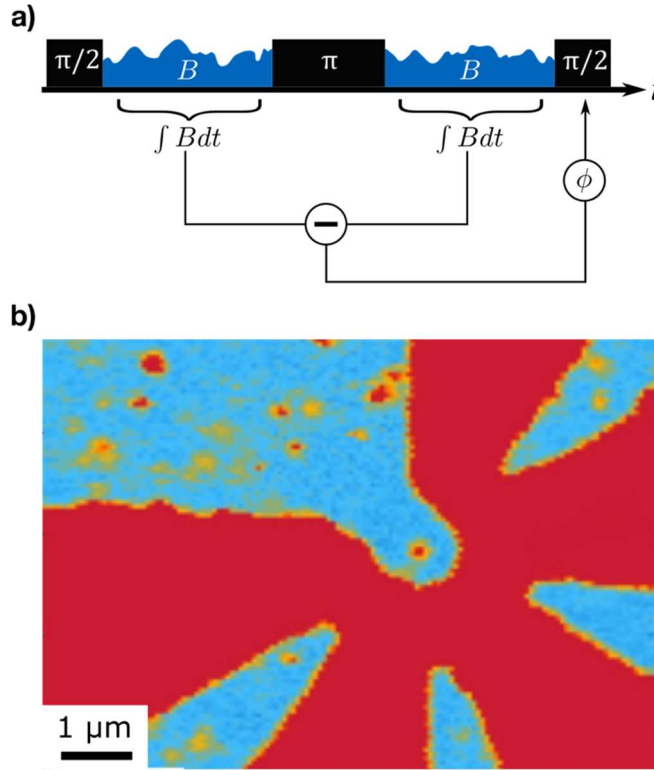


Figure 1: a) Hahn Echo sequence with magnetic field noise during the free evolution times. If the noise is recorded, the phase of the final $\frac{\pi}{2}$ -pulse can be adjusted accordingly to recover the full echo signal. b) Fluorescence scan of diamond sample. A star shaped gold structure embraces a single nitrogen-vacancy center. Both qubit-control and noise field are applied via this structure.

Introduction

Quantum sensing of weak signals often involves exposing a qubit to the signal during a long time [1–3], with noise being a limiting factor for maximum exposure time [4–6]. Manipulating the environment can decrease the noise arising from a few specific sources. For example, cooling to cryogenic temperatures reduces phononic noise [7], although at the cost of increased experimental complexity. Alternatively, the qubit can be controlled to reduce the effect of noise. Dynamical decoupling sequences tailor the spectral sensitivity of the qubit to a narrow frequency range and can drastically improve the coherence time [8–13]. Although they are not restricted to a specific decoherence source, they struggle with heavily fluctuating noise. Quantum error correction can artificially increase the decay constant of a qubit component storing the information by regularly checking the quantum state and actively correcting it [14–16], but analogous to classical memory correction, this requires redundant encoding, which can be infeasible for many systems.

Several state-of-the-art quantum science applications, such as quantum teleportation, rely on processing a quantum measurement during the experiment and feed-forwarding it to the next measurement to, for example, address the right qubit [17], apply a necessary transformation [18] or

determine the appropriate readout basis [19]. In some cases, this is even possible while preventing full projection of the qubit by applying weak measurements for quantum feedback control [20].

In this work, we present feedforward decoupling, an approach that combines dynamical decoupling for constant and slow noise removal, with feedforward control for fast noise suppression. The basic principle is shown in Fig. 1a: We consider a qubit in a coherent superposition in the presence of noise during a free evolution period. The phase ϕ gained depends only on the integral of the noise during that period. If the exact course of noise is known throughout the free evolution, its effect is similar to a known and well-defined phase shift gate applied to the qubit and can be corrected. In order to achieve this, we feed forward for each repetition of the pulse sequence the recorded area of noisy current pulses that act as a classical noise source. We then adapt the phase of the final projection pulse in a Hahn echo experiment to correct for the noise in a feedforward fashion. Our method is similar in spirit to previous work to suppress dephasing by the nuclear bath of a quantum dot, where qubit control was adapted in real-time to a measurement of the nuclear Overhauser field [21]. However, in contrast to this prior work and quantum feedback in general, our feedforward signal is a classical measurement of electric noise rather than a quantum measurement performed by the qubit itself.

Results

We demonstrate this concept in a geometry as displayed in Fig. 1b. A single NV center serves as the qubit system. It is placed in close (μm) proximity to a microfabricated wire in order to enable strong driving [22]. Currents in this wire couple strongly to the NV electron spin, with 1 mA typically translating into 1 G of magnetic field and 2.8 MHz of Zeeman shift. This enables the application of strong control pulses. For instance, a single-qubit phase shift gate can be driven with a Rabi frequency of up to $\Omega_z = 300$ MHz by applying a current of 100 mA. However, the strong coupling also renders the qubit vulnerable to current noise, with 1 mA_{rms} of current fluctuation shortening T_2 to only 50 ns. Active control of currents with this level of noise and bandwidth is technically challenging, which motivated our search for a scheme that replaces it with a mere measurement.

We first apply this paradigm to a challenge of quantum control: to apply a long phase shift gate under the influence of current fluctuations. Unknown fluctuations severely limit the maximum phase that can be gathered coherently. In order to achieve on the order of 100 full phase rotations, we use current measurements and feedforward decoupling to protect the qubit against decoherence from current fluctuations (Fig. 2).

The experimental sequence is displayed in Fig. 2a. We use a slightly altered Hahn echo sequence, where we insert a current pulse during the second free evolution time. Another NV-specific necessity is the projection of the phase onto the NV's z-axis with an additional $\frac{\pi}{2}$ -pulse before readout. The microwave control pulses are provided by a source (Rohde&Schwarz SMIQ06b) that is split by a 90°-splitter (Mini-Circuits ZAPDQ-4+), yielding an in-phase and a quadrature component. These are switched (Mini-Circuits ZASWA-2-50DR+) individually to enable the use of x-phase and y-phase pulses for later experiments. Both components are then combined (Mini-Circuits ZX10-2-442+) into one line and amplified (Mini-Circuits ZHL-16W-43+). The current comes from a direct current source (KORAD KA3005P) that is controlled by a high-side switch (iC-Haus iC-HGP), combined with the microwave signal in a bias tee (Taylor BT-A1080-3), and finally sent towards the gold structure around the NV center.

The current's magnetic field at the NV position leads to a time dependent detuning

$$\Delta(t) = \Delta_0 \cdot I(t)$$

with constant Δ_0 , and thus increases the NV phase by

$$\phi = \int_0^{T_I} \Delta(t) \cdot dt = \Delta_0 \int_0^{T_I} I(t) \cdot dt$$

inducing an oscillation of the NV spin with increasing integrated current (Fig. 2b and 2c). The oscillations have a contrast of less than unity because of intrinsic decoherence during the Hahn echo.

For each experimental repetition, we measure and integrate the respective current before correlating it to the qubit readout result. A differential probe (Yokogawa 701920) measures the current flow by monitoring the voltage drop over a 50 Ω resistor that is in series with the current application structure. An oscilloscope (Spectrum M4i.4451-x8) with 500 MS/s and a 14-bit digital resolution is recording the voltage for every repetition, allowing us to correlate each readout result with its preceding current pulse. Specifically, NV photons collected during the readout pulse are registered and binned by their measured pulse area $\int_0^{T_I} I(t) \cdot dt$. In this way, photons will contribute to the signal at the actual value of pulse area, not the nominal setpoint chosen by pulse duration and/or current amplitude.

The recorded oscillations in Figure 2 show a decay limited by the intrinsic constant $T_2 = (1.4 \pm 0.1) \mu\text{s}$. In other words, the original signal drops to $1/e$ over 130 ± 9 full oscillations, corresponding to an infidelity per π -pulse of $5 \cdot 10^{-2}$. This measurement also provides a calibration of $\Delta_0 = (9.48 \pm 0.08) \cdot \frac{\text{rad}}{\text{mA} \cdot \mu\text{s}}$.

We now focus on a different challenge: to recover an echo envelope in the presence of strong fluctuations of the current by applying feedforward decoupling (Fig. 3). This scenario is representative for all measurements that involve strong fields or control pulses, such as imaging experiments that require a strong magnetic field gradient [23]. As before, we perform an echo decay measurement, which is perturbed by a current pulse during the second free evolution period. The current pulses are of random duration ranging from 0 ns to τ with an amplitude of 3.50 ± 0.02 mA and are measured in each experimental repetition. The measured current is converted into a phase by the previously calibrated Δ_0 and fed forward to the phase of the final $\frac{\pi}{2}$ -pulse in order to maximize the echo signal. This step could either be performed by real-time electronic processing or can be emulated by post-selection, which is the approach we choose for this study. Specifically, we alternate the phase of the final $\frac{\pi}{2}$ -pulse between subsequent repetitions (Fig. 3a), implementing alternating readout of the observables σ_x and σ_y . We then discard those measurements that do not match the feedforward phase computed above (Fig. 3b).

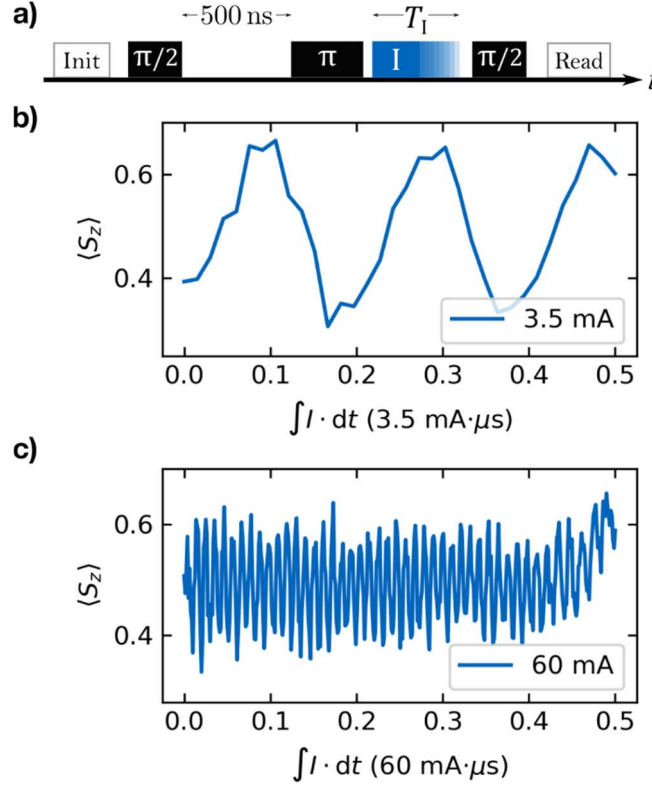


Figure 2: a) Measurement sequence. A Hahn echo sequence with fixed free evolution times of 500 ns is applied, reducing the oscillation amplitude to 20 % of the full Rabi oscillation contrast. During the second free evolution time, a current pulse of fixed amplitude I_0 and varying duration T_I is applied. b) + c) Oscillation of the spin qubit z-component depending on the current induced phase for currents with an amplitude of 3.5 mA (b) and 60 mA (c). The oscillation frequency scales with the amplitude.

For a better understanding, we use the Bloch sphere visualization for the gathered phase during the second free evolution period, so that the phase corresponds to the azimuthal angle ϕ . In more detail, we discretize the gathered phase into four quadrants (Fig. 3b), corresponding to maximum positive z-component after a $\frac{\pi}{2}$ -pulse with x- or y-phase (x+, illustrated in Fig. 3c, and y+), and maximum negative z-component after a $\frac{\pi}{2}$ -pulse with x/y-phase (x-/y-). The phase of the final $\frac{\pi}{2}$ -pulse is alternating between x and y and we only keep the measurement if the combination of gathered qubit phase and the phase of the final $\frac{\pi}{2}$ -pulse maximizes the absolute of the qubits final z-component and thus the signal contrast. The dark blue curve in Fig. 3d shows the measurement outcome in the presence of the current noise of the random-duration current pulses before without post-selection. The result is an exponential decay with $T_2 = (55 \pm 13)$ ns, which is much shorter than the measured decay of the echo in the absence of any current pulse (Fig. 3d, light blue curve), where the decay constant is $T_2 = (389 \pm 133)$ ns. The red and green curves are the post-selected results of our feedforward decoupling method for x- and y-projection pulses, respectively. The method corrects the perturbing effect of the random-duration current pulses, increasing the coherence time sevenfold to $T_2 = (366 \pm 133)$ ns, reaching the value of the unperturbed measurement within the measurement accuracy.

We now extend feedforward decoupling to a scheme, which does not require pre-calibration of the qubit response and instead learns the value of Δ_0 on the fly. We record and save the free evolution duration τ , the integrated current $\int I dt$, the projection pulse phase, still only allowing x and y, and the

readout result for every repetition (Fig. 4). Finally, we correct for the decoherence caused by the current noise in post-processing.

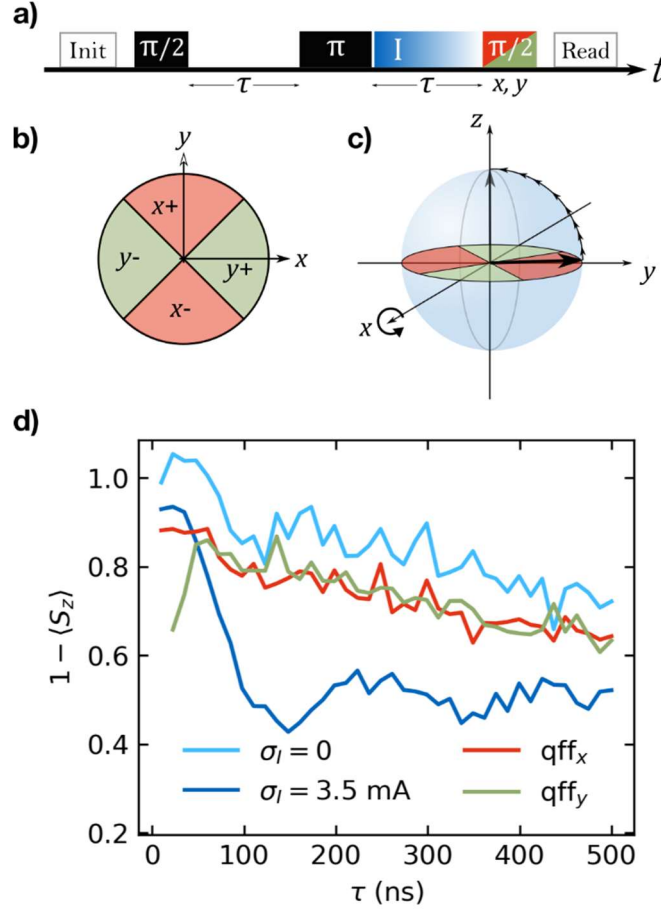


Figure 3: a) A Hahn echo sequence with variable free evolution time τ . During the second free evolution time, a current pulse of random length is applied. The phase of the final $\frac{\pi}{2}$ -pulse before readout is alternated between x and y . b) Top view of a Bloch sphere equatorial plane. We divide the unit circle into four quadrants, each representing a potential projection phase to maximize the signal amplitude $1 - \langle S_z \rangle$ for a given qubit state at 2τ . A state in a red quadrant requires a final $\frac{\pi}{2}$ -pulse with x -phase, a green one a $\frac{\pi}{2}$ -pulse with y -phase to maximize the signal. c) Bloch sphere with the quadrants from b) indicated. The bold black arrow depicts a possible qubit state before the last $\frac{\pi}{2}$ -pulse in a red quadrant. A $\frac{\pi}{2}$ -pulse with x -phase invokes the indicated rotation, eventually bringing the qubit state parallel to the z -axis. A pulse with y -phase would invoke a rotation around the y -axis, which in this case would yield barely any contrast. d) Measurement results of the sequence shown in a). The light blue graph is the result in absence of noise, decaying with constant $T_2 = (389 \pm 133) \text{ ns}$. The dark blue graph shows the result in the presence of noise without any post-selection, leading to the short decaying constant $T_2 = (55 \pm 13) \text{ ns}$. The red (green) graph, derived from the measured data by feedforward decoupling, neglects all results but those where an x -phase (y -phase) projection pulse was applied on the qubit system in one of the red (green) quadrants of b).

The triangular shape of the 2d-plot in the top left panel of Fig. 4 is associated with the boundary condition $T_I \leq \tau$, which limits the integrated current to low values for short τ . Plotting oscillation amplitudes against τ , shown below the 2d-plot, provides the expected echo decay. The projection along the $\int I dt$ -axis, shown to the right of the 2d-plot, exhibits a phase oscillation comparable to those in Figs 2b) and c). From this data, we can extract the calibration analogously to before and apply the same post-selected feedforward decoupling correction. We note that the coupling to the current and the

oscillation frequency differ from the data of Fig. 2 as this experiment was conducted on a different NV center.

This self-learning approach is faster than the pre-calibration approach of Figs 2 and 3, since every measurement contributes simultaneously to both the echo envelope and the calibration of the qubit response. This also implies that the accuracy of the post-measurement calibration is the same as for the previous method: N measurements provide N data points for the calibration curve in both cases. Further, instead of the simple quadrant calibration introduced in Fig. 3b), the post-measurement calibration allows for example to fit a sine curve for every value of τ . This performs better especially for boundary cases, where ϕ lies close to the quadrant boundaries in Fig. 3b). In future work, machine learning and Bayesian techniques could further improve efficiency [21].

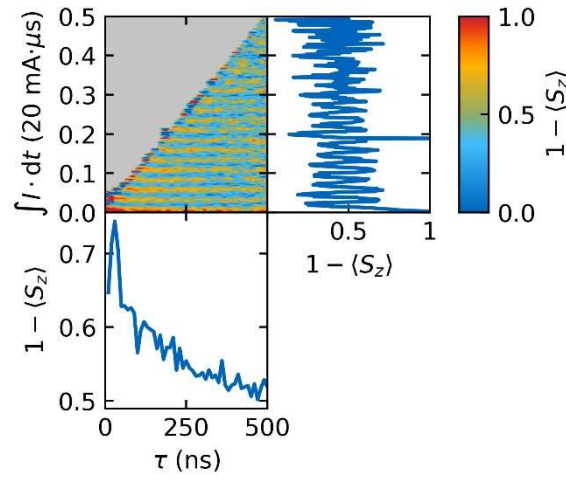


Figure 4: Post-measurement calibration. The measurement result for different τ and T_1 is shown in the 2d-plot of the top left panel. The projection of the data onto the integrated-current axis, shown in the top right panel, exhibits a phase oscillation, corresponding to the one used for pre-calibration. It is used for a post-measurement calibration. The oscillation amplitude for each τ , shown in the bottom left panel, shows the expected echo decay.

We now turn to a benchmark of our method. Similar to the measurement in Fig. 2, we fix the free evolution period of an echo to $32 \mu\text{s}$ and sweep the duration of a current pulse with nominally constant

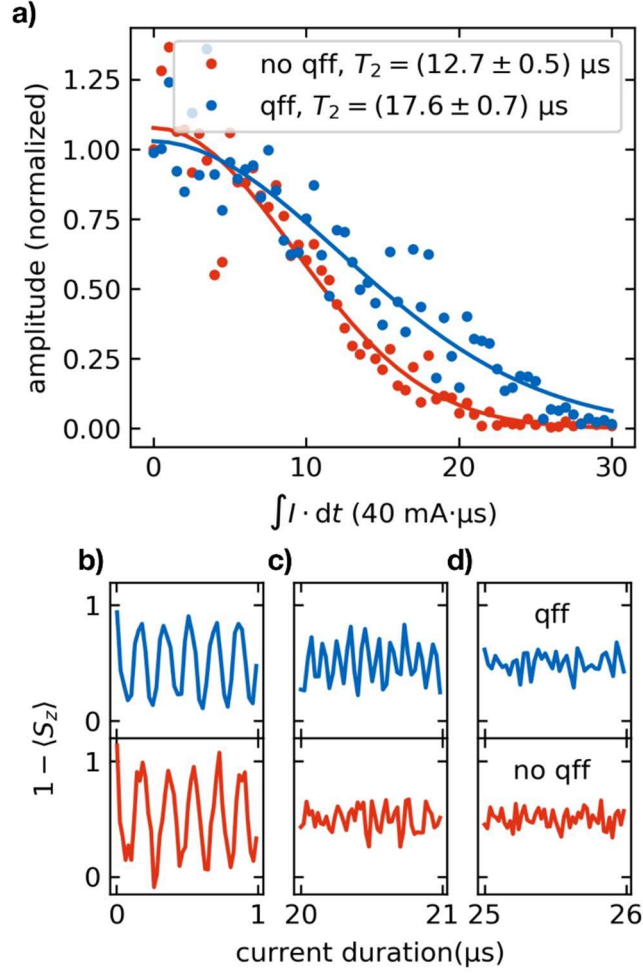


Figure 5: Echo benchmark. The duration of a current pulse is swept during the second free evolution period of an echo with fixed free evolution time of $32 \mu\text{s}$ (compare Figure 2a). We compare the decay of the resulting oscillation graph with (blue) and without correction (red). The current pulse is nominally set to 40 mA and swept from 5 ns to $30 \mu\text{s}$. a) The qff correction extends the decay constant T_2 from $(12.7 \pm 0.5) \mu\text{s}$ to $(17.6 \pm 0.7) \mu\text{s}$. b), c) and d) Exemplary comparisons of the oscillations with and without qff correction. The most dramatic difference can be seen in c), where the qff technique clearly recovers an oscillation that would otherwise be lost.

amplitude. We compare the resulting oscillation amplitude over time, once without any correction and once corrected for current fluctuations as described above. The echo decays noticeably faster without correction. Using the measured amplitude and pulse duration for correction, we can extend the decay constant T_2 from $(12.7 \pm 0.5) \mu\text{s}$ to $(17.6 \pm 0.7) \mu\text{s}$ in our experiment (Fig. 5a). Figs 5b – 5d show the recorded oscillation, zoomed in for certain time periods. Both curves behave the same for very short (Fig. 5b) and very long current (Fig. 5d) pulses. However, there is a significant difference at intermediate pulse lengths (Fig. 5c). With feedforward decoupling, there is still a significant oscillation visible, while the uncorrected measurement has already decayed to pure noise. Given an oscillation frequency of $\Delta\omega_z = 10 \text{ MHz}$, our technique enables us to perform 38% more full oscillations than the classical noise of our current source allows.

Discussion

Feed-forward decoupling succeeds in mitigating noise from fluctuating control currents in all three different schemes tested in this study. Quantitatively, the improvement afforded is weaker than expected. For all our experiments, the infidelity is approximately 10^{-2} . In an imaging experiment, this would limit localization precision to approximately 25 nm. This infidelity is much higher than the ultimate limit, which is set by the digitization noise of the oscilloscope. With a 14-bit digitization accuracy and typically 25 measurements per π phase shift gate, future experiments reaching this limit should be able to reach an infidelity as low as 10^{-5} .

The most plausible interpretation of this discrepancy is that the method is successful in eliminating current noise, but that current noise is not the dominating source of dephasing in our present device. There are several other effects that could provide such a source. One possible candidate is heat expansion of the conductors. As the conductors have a cross-section of $\sim 1 \mu\text{m}^2$, a fluctuating expansion of 2.5% would displace the current by 25 nm and explain the measured infidelity. However, this would imply a temperature change of more than 1000 K, which seems unlikely. Another problem might be the granularity of the electroplated gold [24], which might lead to different conduction channels of our gold structures depending on the temperature and power throughout the applied pulses. An uncertainty of only 25 nm of the current path in the $1 \mu\text{m}$ wide structure would already suffice to explain the infidelity of our experiments. Measurements on devices with evaporated monocrystalline gold structures [25], which should be less susceptible to this problem, will be the subject of future work.

Even if this limitation cannot be overcome, we foresee several short-term applications for feedforward decoupling. One direction is Fourier imaging, where the present performance would be sufficient to determine the position of two optically unresolvable nitrogen-vacancy centers with a resolution of 25 nm, comparable to current state-of-the-art approaches [23,26]. Another direction are quantum sensing and computation schemes that involve simultaneous manipulation of an electron spin and nuclear qubits [3]. Here, nuclear gates require strong pulses in the MHz regime, and magnetic crosstalk to the electron spin is a source of dephasing. Removing this limitation with our feedforward scheme could thus expand the range of usable protocols for these experiments.

This work has been supported by the European Union (Horizon 2020 research and innovation programme, grant agreement No 820394 (ASTERIQS)), as well as by the Deutsche Forschungsgemeinschaft (DFG, German Research Foundation) under the German Excellence Strategy – EXC-2111 – 390814868, Emmy Noether grant RE3606/1-1 and the DFG-NFSC program (RE3606/3-1).

- [1] G. de Lange, T. van der Sar, M. Blok, Z.-H. Wang, V. Dobrovitski, and R. Hanson, *Scientific Reports* **2**, 382 (2012).
- [2] T. Staudacher, F. Shi, S. Pezzagna, J. Meijer, J. Du, C. A. Meriles, F. Reinhard, and J. Wrachtrup, *Science* **339**, 561 (2013).
- [3] H. J. Mamin, M. Kim, M. H. Sherwood, C. T. Rettner, K. Ohno, D. D. Awschalom, and D. Rugar, *Science* **339**, 557 (2013).
- [4] J. Yoneda, K. Takeda, T. Otsuka, T. Nakajima, M. R. Delbecq, G. Allison, T. Honda, T. Kodera, S. Oda, Y. Hoshi, N. Usami, K. M. Itoh, and S. Tarucha, *Nature Nanotech* **13**, 102 (2018).
- [5] Y. Romach, C. Müller, T. Uden, L. J. Rogers, T. Isoda, K. M. Itoh, M. Markham, A. Stacey, J. Meijer, S. Pezzagna, B. Naydenov, L. P. McGuinness, N. Bar-Gill, and F. Jelezko, *Phys. Rev. Lett.* **114**, 017601 (2015).

- [6] P. Jamonneau, M. Lesik, J. P. Tetienne, I. Alvizu, L. Mayer, A. Dréau, S. Kosen, J.-F. Roch, S. Pezzagna, J. Meijer, T. Teraji, Y. Kubo, P. Bertet, J. R. Maze, and V. Jacques, *Phys. Rev. B* **93**, 024305 (2016).
- [7] K. Saeedi, S. Simmons, J. Z. Salvail, P. Dluhy, H. Riemann, N. V. Abrosimov, P. Becker, H.-J. Pohl, J. J. L. Morton, and M. L. W. Thewalt, *Science* **342**, 830 (2013).
- [8] Ł. Cywiński, R. M. Lutchyn, C. P. Nave, and S. Das Sarma, *Phys. Rev. B* **77**, 174509 (2008).
- [9] J. H. Shim, I. Niemeyer, J. Zhang, and D. Suter, *EPL* **99**, 40004 (2012).
- [10] G. de Lange, D. Ristè, V. V. Dobrovitski, and R. Hanson, *Phys. Rev. Lett.* **106**, 080802 (2011).
- [11] S. Kotler, N. Akerman, Y. Glickman, A. Keselman, and R. Ozeri, *Nature* **473**, 61 (2011).
- [12] J. Bylander, S. Gustavsson, F. Yan, F. Yoshihara, K. Harrabi, G. Fitch, D. G. Cory, Y. Nakamura, J.-S. Tsai, and W. D. Oliver, *Nature Physics* **7**, 565 (2011).
- [13] N. Bar-Gill, L. M. Pham, C. Belthangady, D. Le Sage, P. Cappellaro, J. R. Maze, M. D. Lukin, A. Yacoby, and R. Walsworth, *Nature Communications* **3**, 858 (2012).
- [14] N. Ofek, A. Petrenko, R. Heeres, P. Reinhold, Z. Leghtas, B. Vlastakis, Y. Liu, L. Frunzio, S. M. Girvin, L. Jiang, M. Mirrahimi, M. H. Devoret, and R. J. Schoelkopf, *Nature* **536**, 441 (2016).
- [15] T. Unden, P. Balasubramanian, D. Louzon, Y. Vinkler, M. B. Plenio, M. Markham, D. Twitchen, A. Stacey, I. Lovchinsky, A. O. Sushkov, M. D. Lukin, A. Retzker, B. Naydenov, L. P. McGuinness, and F. Jelezko, *Phys. Rev. Lett.* **116**, 230502 (2016).
- [16] M. Hirose and P. Cappellaro, *Nature* **532**, 77 (2016).
- [17] N. Sinclair, E. Saglamyurek, H. Mallahzadeh, J. A. Slater, M. George, R. Ricken, M. P. Hedges, D. Oblak, C. Simon, W. Sohler, and W. Tittel, *Phys. Rev. Lett.* **113**, 053603 (2014).
- [18] X.-S. Ma, T. Herbst, T. Scheidl, D. Wang, S. Kropatschek, W. Naylor, B. Wittmann, A. Mech, J. Kofler, E. Anisimova, V. Makarov, T. Jennewein, R. Ursin, and A. Zeilinger, *Nature* **489**, 269 (2012).
- [19] R. Prevedel, P. Walther, F. Tiefenbacher, P. Böhi, R. Kaltenbaek, T. Jennewein, and A. Zeilinger, *Nature* **445**, 65 (2007).
- [20] R. Vijay, C. Macklin, D. H. Slichter, S. J. Weber, K. W. Murch, R. Naik, A. N. Korotkov, and I. Siddiqi, *Nature* **490**, 77 (2012).
- [21] M. D. Shulman, S. P. Harvey, J. M. Nichol, S. D. Bartlett, A. C. Doherty, V. Umansky, and A. Yacoby, *Nature Communications* **5**, (2014).
- [22] G. D. Fuchs, V. V. Dobrovitski, D. M. Toyli, F. J. Heremans, and D. D. Awschalom, *Science* **326**, 1520 (2009).
- [23] K. Arai, C. Belthangady, H. Zhang, N. Bar-Gill, S. J. DeVience, P. Cappellaro, A. Yacoby, and R. L. Walsworth, *Nature Nanotech* **10**, 859 (2015).
- [24] C.-W. Baek, Y.-K. Kim, Y. Ahn, and Y.-H. Kim, *Sensors and Actuators A: Physical* **117**, 17 (2005).
- [25] U. Höpfner, H. Hehl, and L. Brehmer, *Applied Surface Science* **152**, 259 (1999).
- [26] I. Jakobi, P. Neumann, Y. Wang, D. B. R. Dasari, F. E. Hallak, M. A. Bashir, M. Markham, A. Edmonds, D. Twitchen, and J. Wrachtrup, *Nature Nanotech* **12**, 67 (2017).